Stress Wave Propagation through Cohesive Soil

AUTHOR(S):

AKAI, Koichi; OKA, Fusao; KITA, Kenji

CITATION:

AKAI, Koichi ...[et al]. Stress Wave Propagation through Cohesive Soil. Memoirs of the Faculty of Engineering, Kyoto University 1978, 40(3): 152-168

ISSUE DATE:

1978-07

URL:

http://hdl.handle.net/2433/281073

Stress Wave Propagation through Cohesive Soil

By

Koichi AKAI*, Fusao OKA* and Kenji KITA*

(Received March 30, 1978)

Abstract

Generally, there exist an inelastic deformation and an energy dissipation during the stress wave propagation through cohesive soil. In order to describe these characteristics, the authors proposed the constitutive equation of normally consolidated clay. The phenomenological nature of the parameters involved in the stress-strain relation was investigated in detail by using the triaxial test results and the stress wave propagation test results. In these test the pore water pressure was measured and its value was compared with the calculated result by using the constitutive equation of clay. As a result, the proposed stress-strain relation was very effective for interpreting the behavior of cohesive soil.

1. Introduction

Generally, it is well known that there exist an inelastic deformation and an energy dissipation during the stress wave propagation through cohesive soil. In order to describe these characteristics, many researchers have carried out experimental studies and have proposed various mechanical models of soil. For example, Seaman[1] proposed the viscoelastic compacting model and the S-hysteretic model. Comparing the experimental results, he concluded that the tan δ-model which exhibited a frequency independent dissipation well described the attenuation of peak stress during the wave propagation in clay. Vey and Strauss[2] carried out the stress wave propagation test through clay, and proposed the non-linear Voigt model for clay.

However, the behavior of pore water pressure during the stress wave propagatian has seldom been examined. In this paper, the authors tried to measure the pore water pressure during the stress weve propagation through cohesive soil, and estimated the value of the pore water pressure by using the stress-strain relation of

* Department of Transportation Engineering

cohesive soil proposed by authors.

In section 2, the experimental results of the stress wave propagation through saturated cohesive soil by a triaxial special cell connected with a shock tube is shown. In particular, the emphasis is on the developement of the pore water pressure. In section 3, the proposed stress-strain relation of cohesive soil is examined by the strain-rate controlled triaxial compression test, neglecting the viscoelastic effect. In section 4, using the results of section 3, the one-dimensional stress wave propagation through cohesive soil is analytically studied by the method of characteristics.

2. Experimental Study

A one-dimensional stress wave propagation test was carried out by using the special triaxial cell in connection with the air shock tube[3]. The soil specimen was prepared from Fukakusa dry clay which was sieved by 400μ net, kneaded with water and consolidated at a surcharge of 2.0kg/cm^2 for about 40 days. Soil specimen with a length about 130 cm and a diameter of 7.5 cm was assembled from four pieces of soil column. Pre-consolidation pressure was from 0.6 to 0.85kg/cm^2. The physical properties of the soil are shown in Table 1. The measuring system consists of a soil stress gauge, a pore water pressure transducer, an amplifier and synchroscopes.

Table 1 Physical properties of soil.

Specific gravity	2.67
LL	50.5-60.0%
PL	25.5-31.9%
PI	21.6-34.5
Uniformity coefficient	2.85
Water content	36.7-42.5%
Bulk density	1.72-1.83g/cm^3

Pore water pressure is developed under the undrained condition during the stress wave propagation. It is necessary to measure pore water pressure to investigate the soil behavior in terms of effective stress. To date, however, data of pore water pressure during the stress wave propagation have been hardly obtained because of the difficulties in the measuring system. In this experiment, the pore water pressure was measured by using a pressure transducer with a needle-like tube filled with porous stone as shown in Fig. 1. Fig. 2 shows the obtained form of pore water pressure where the peak pressure decreases slightly and the rise time increases with travelling time, similar to the form of the stress. Typical forms of the stress wave and the pore

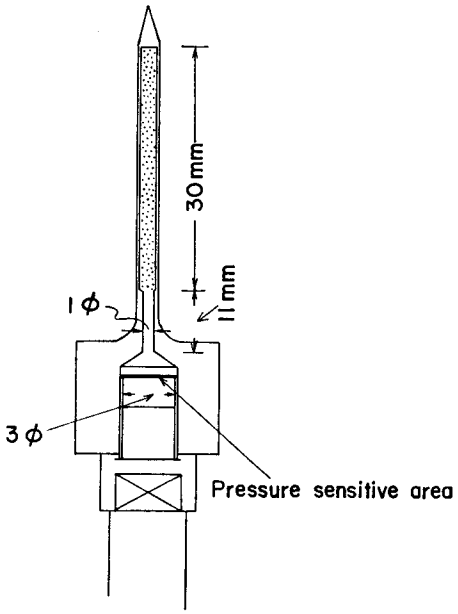

Fig. 1 Equipment of measuring the pore water pressure.

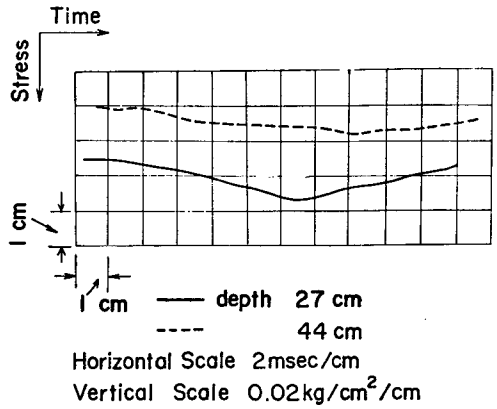

Fig. 2 Pore pressure-time profile.

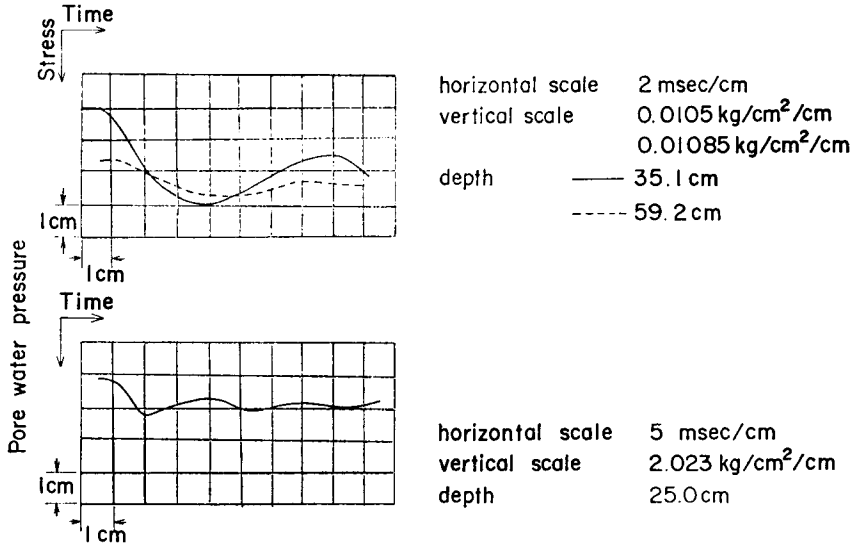

Fig. 3 Pore pressure and stress-time profiles.

Table 2 Measured value of peak stress and peak pore water pressure.

Test No.	σ'_{me} (kg/cm²)	Soil pressure			Pore Water Pressure		
		q_{max} (kg/cm²)	rise time (msec)	depth (cm)	u_{max} (kg/cm²)	rise time (msec)	depth (cm)
1	0.6	0.164	7.6	86.2	0.051	12.0	27.0
		0.139	8.8	113.0	0.024	16.0	44.0
2	0.6	0.175	6.6	86.2	0.051	11.2	27.0
		0.142	7.5	113.0	0.016	14.0	44.0
3	1.1	0.242	7.2	37.5	0.010	8.0	43.5
		0.232	6.5	68.0	0.008	8.8	58.0
4	0.5	0.247	10.9	22.8	0.0167	12.9	22.8
5	1.2	0.315	6.9	22.0	0.0347	5.0	22.0
6	0.7	0.184	9.4	17.5	0.0183	10.4	17.5
7	1.2	0.257	6.4	17.5	0.0107	11.4	17.5
8	1.0	0.299	5.0	18.9	0.0104	3.6	18.9

σ'_{me} consolidation pressure

water pressure are shown in Fig. 3. Table 2 summarizes the measured value of the peak stress and the peak pore water pressure. It may be noted from tests No. 1, 2 and 3 that a peak value of pore water pressure attenuates more rapidly than that of stress. The rate of increase of the rise time of pore water pressure is greater than that of the stress.

3. Stress-Strain Relation of Cohesive Soil

The authors[4),5)] proposed the stress-strain relation of normally consolidated cohesive soil. Cohesive soil is regarded as a viscoelastic-viscoplastic body, which is given by

$$\frac{d\varepsilon_{ij}}{dt}=\gamma_1\dot{s}_{ij}+\gamma_2\dot{\sigma}'_m\frac{1}{3}\delta_{ij}+(2b^{(2)}s_{ij}-2\tau^{(2)}e^{vp}_{ij})$$
$$+(3a^{(2)}\sigma'_m-3\tau^{(1)}\varepsilon^{vp}_{kk})\delta_{ij}+\frac{s_{ij}}{\sqrt{2J_2}}\beta_1$$
$$+\frac{1}{3}\delta_{ij}\{M^*-\frac{\sqrt{2J_2^{(s)}}}{\sigma_m^{(s)}}+M^*\ln(\sigma'_m/\sigma'^{(s)}_m)\}\beta_2 \qquad (1)$$

The index (s) denotes the point on the static stress path having an inelastic strain equal to the present point on the dynamic stress path. The static stress-strain relation is given by Roscoe's original theory extended to a three-dimensional case[6)]. In

Eq. (1), ε_{ij} is the strain tensor, e_{ij}^{ve} the deviatoric viscoelastic strain tensor, s_{ij} the deviatoric stress tensor, σ'_m the mean effective stress, J_2 the second invariant of s_{ij} and M^* the value of $\sqrt{2J_2}/\sigma'_m$ at critical state.

In the case of a conventional axi-symmetric compression,

$$s_{11}=\frac{2}{3}(\sigma'_{11}-\sigma'_{22})=\frac{2}{3}q, \quad e_{11}=\varepsilon_{11}, \quad \sigma'_m=\frac{1}{3}\sigma'_{kk},$$

$$s_{ij}/\sqrt{2J_2}=\sqrt{\frac{2}{3}}, \quad \dot{\varepsilon}'_{11}=\frac{2}{3}(\dot{\varepsilon}_{11}-\dot{\varepsilon}'_{22}) \tag{2}$$

where q is the deviator stress and e_{ij} the deviatoric strain tensor.

From Eq. (1), the stress-strain relation in undrained axisymmetric triaxial compression is expressed by

$$\dot{e}_{11}=\gamma_1\dot{s}_{11}+\sqrt{\frac{2}{3}}\beta_1+\left(\frac{4}{3}b^{(2)}q-2\tau^{(2)}e_{11}^{ve}\right) \tag{3}$$

$$\sqrt{\frac{2}{3}}\beta_1=C_1\exp\left\{\frac{m}{\sigma'_{me}}(q-q^{(s)})\right\}, \quad \dot{\varepsilon}_{11}^{vp}=\sqrt{\frac{2}{3}}C_0\exp\left\{\frac{m(\varepsilon_{11}^{ve})}{\sigma'_{me}}(q-q^{(s)})\right\} \tag{4}$$

If the viscoelastic volume change is zero, taking the condition of $\varepsilon_{kk}=0$ into consideration, it will be expressed as

$$\gamma_2\dot{\sigma}'_m+\beta_2\left\{M^*-\frac{\sqrt{2J_2}^{(s)}}{\sigma'^{(s)}_m}+M^*\ln(\sigma'_m/\sigma'^{(s)}_m)\right\}=0 \tag{5}$$

$$\dot{\sigma}'_m=-\frac{1}{\gamma_2}\beta_2\left\{M^*-\frac{\sqrt{2J_2}^{(s)}}{\sigma'^{(s)}_m}+M^*\ln(\sigma'_m/\sigma'^{(s)}_m)\right\} \tag{6}$$

$(\beta_2=\beta_1)$

The authors already examined the effectiveness of Eq. (3) in the triaxial compression test, but Eq. (5) was not examined. In this section, the effectiveness of Eq. (6) in the strain-rate constant triaxial compression test and the stress wave propagation test is discussed. Under the condition that the strain-rate is 0.01 %/min. to 4 %/min., since the viscoelastic nature of soil can be neglected, Eq (3) becomes

$$\dot{e}_{11}=\gamma_1\dot{s}_{11}+\sqrt{\frac{2}{3}}\beta_1$$

$$=\frac{1}{E'}\dot{q}+C_1\exp\left(\frac{m}{\sigma'_{me}}(q-q^{(s)})\right) \tag{7}$$

In Eq. (7), E' is Young's modulus and σ'_{me} is the consolidation pressure.

Fig. 4 represents the effective stress path under the triaxial compression test on normally consolidated clay carried out by Richardson and Whitman[7]. This figure indicates that the strain-rate greatly influences the effective stress path and the pore water pressure development. These effects of strain-rate to stress path will be discussed on the basis of the authors' theory. Figs. 5 and 6 show a theoretical effective stress path and a stress-strain relation under the strain-rate controlled triaxial

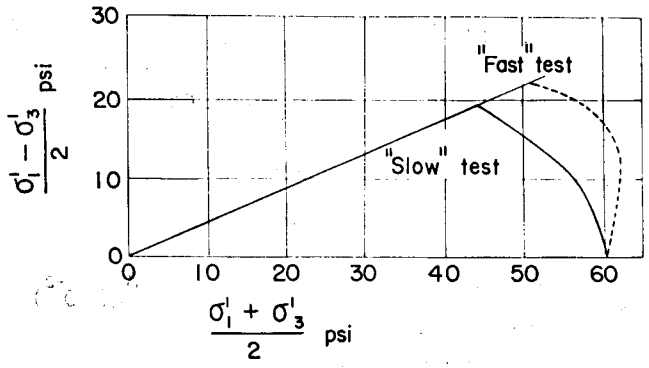

Fig. 4 Average stress path under triaxial compression test on a normally consolidated clay.[7]

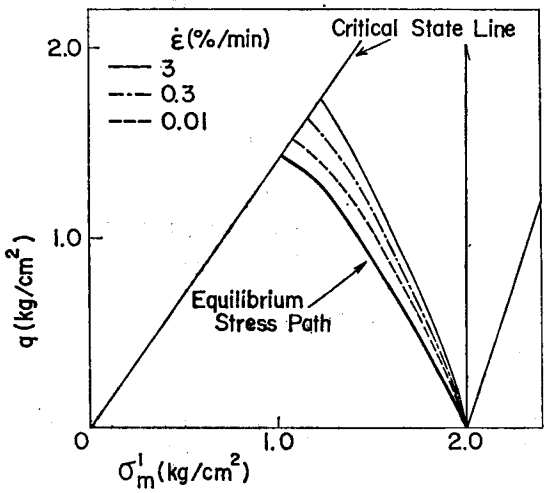

Fig. 5 Calculated results of stress path of strain-rate constant triaxial compression test.

compression test on normally consolidated clay, calculated by using Eqs. (5) and (7). The calculation was carried out by using Runge-Kutta's method, in which the relation $\gamma_2=\kappa/\{(1+e_o)\sigma_m'\}$ was assumed, considering the swelling curve, the e-lnσ_m' line. From these figures, it may be noted that the effect of strain rate can be reasonably assessed by the authors' theory. In Fig. 5, the equilibrium stress path can be given by Roscoe's original theory[6]. Finally, it may be concluded that the dynamic stress-strain-pore pressure relation of normally consolidated clay can be completely described by solving Eqs. (5) and (7) at the same time.

Fig. 7 shows the relation between the deviator stress and the rate of increase of

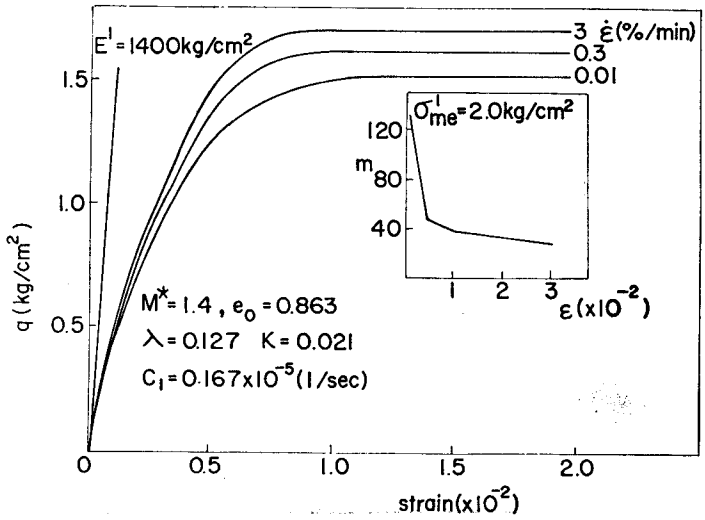

Fig. 6 Calculated results of stress-strain relation of strain-rate constant triaxial compression test.

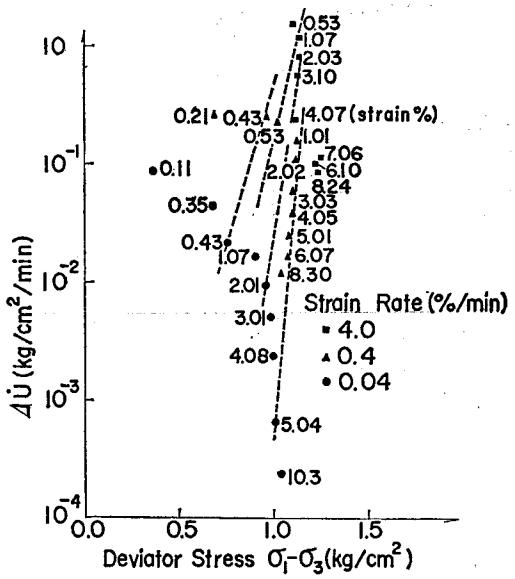

Fig. 7 Relationship between rate of excess pore water pressure and deviator stress.

the pore water pressure due to an effect of dilatancy, which has been obtained from the triaxial test with a constant strain rate. From this figure, a phenomenological relation may be deduced:

$$\log \Delta \dot{u} = \log \Delta \dot{u}_o + \bar{\delta}(\sigma_1 - \sigma_3) \qquad (8)$$

where, $\bar{\delta}$ denotes the slope of the line in Fig. 7 and depends on the magnitude of strain, and u is the pore water pressure. Under the condition of a triaxial compression test, we have

$$\sigma'_m=\sigma'_{me}+\frac{1}{3}(\sigma'_{11}-\sigma'_{33})-u \tag{9}$$

Therefore, the time rate of a mean effective stress is given by

$$\dot{\sigma}'_m=\overline{\sigma'_{me}+\frac{1}{3}q-u}=\overline{\frac{1}{3}q-u}=-\Delta\dot{u} \tag{10}$$

where, $\Delta\dot{u}$ is the rate of increase of the pore water pressure due to the dilatancy. Substituting Eq. (10) into Eq. (6),

$$\Delta\dot{u}=\Delta\dot{u}_0\exp\left(\frac{m}{\sigma'_{me}}q\right) \tag{11}$$

so that $$\ln\Delta\dot{u}=\ln\Delta\dot{u}_0+\frac{m(\varepsilon_{11})}{\sigma'_{me}}q \tag{12}$$

it becomes evident that this relation is equivalent to Eq. (8).

Now, we will perform a parametric study and consider a correlation of the parameters, one m/σ'_{me} for the pore water pressure development expressed by Eq. (12) which corresponds to the empirical relation Eq. (8) and the other for the shear stress and strain relation expressed by Eq. (4) corresponding to the empirical relation given by

$$q(\varepsilon_{11},\dot{\varepsilon}_{11})-q(\varepsilon_{11},\dot{\varepsilon}_{11(0)})=\alpha(\varepsilon_{11})\log(\dot{\varepsilon}_{11}/\dot{\varepsilon}_{11(0)})^{8)} \tag{13}$$

It should be again noted that Eqs. (4) and (12) are expressed in natural logarithmic form, while the empirical equations are expressed in common logarithmic form.

From the experimental results, $\bar{\delta}$ and α can be determined as 7.8 at $\varepsilon=1.07$ % from Fig. 7, and 10 from Fig. 8, respectively. Taking the correspondence Eq.

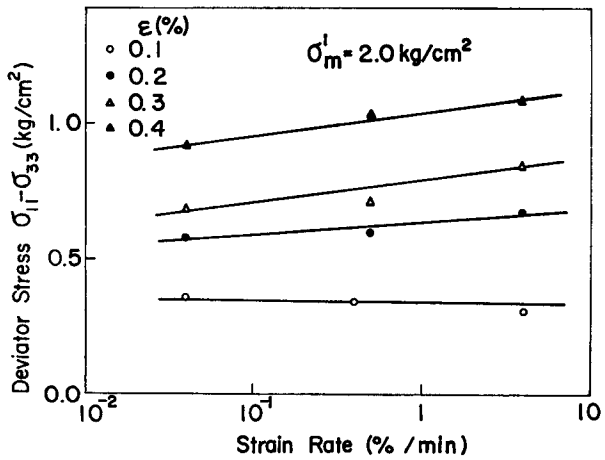

Fig. 8 Relationship between deviator stress and logarithm of strain rate.

(8) to Eq. (12) and Eq. (13) to Eq. (4) into consideration, the value of m/σ'_{me} in Eq. (12) becomes 18 (7.8×2.303), and the value in Eq. (4) becomes 23(10×2.303). Consequently, a conclusion may then be drawn that the parameters which have been individually determined from the pore water pressure development and the shear stress-strain relation are identical to each other with a relatively high correlation. That is to say, although an assumption has been made that functions β_1 and β_2 are identical and relevant, equations for the pore water pressure and the shear stress-strain relation have been deduced. It could be noted from the parametric study discussed above that this assumption is moderately consistent with the experimental results.

On the other hand, Matsui *et al.*[9] deduced the phenomenological relation governing the development of excess pore water pressure due to a repeated loading, using Singh & Mitchell's method.[10]

$$\ln \Delta \dot{u} = \ln \Delta \dot{u}(t, \tau_{do}) + \alpha' \tau_d \tag{14}$$

where τ_d is the maximum shear stress and $\Delta \dot{u}$ the rate of increase of the pore water pressure. Since τ_d exactly corresponds to q, Eq. (13) is also equivalent to Eq. (12).

4. One-dimensional Stress Wave Propagation through Cohesive Soil

We shall discuss the one-dimensional wave propagation through cohesive soil, which is described by Eqs. (3) and (6). Eqs. (3) and (6) are rewritten by

$$\frac{\partial \varepsilon_{11}}{\partial t} = \frac{1}{E'} \frac{\partial q}{\partial t} + C_1 \exp\left(\frac{m}{\sigma'_{me}} (q - q^{(s)}) \right) + (\mu q - E \mu \varepsilon_{11}^{ve}) \tag{15}$$

$$\frac{\partial \sigma'_m}{\partial t} = -\frac{C_2}{\tau_2} \exp\left(\frac{m}{\sigma'_{me}} (q - q^{(s)}) \right) \tag{16}$$

where $\mu = \frac{4}{3} b^{(2)}$ and $E = \frac{3\tau^{(2)}}{2b^{(2)}}$.

The bar wave propagation can be observed under the condition that the lateral displacement is not confined and that the wave length is very small compared to the diameter of the bar. The boundary condition is given by the stress condition. The stress condition is under the wave propagation test using the special triaxial cell, and is equal to the strain-rate controlled triaxial compression test which is given by

$$\sigma_{ij} = \begin{pmatrix} \sigma_{11}, & 0, & 0 \\ 0, & \sigma_{22}, & 0 \\ 0, & 0, & \sigma_{33} \end{pmatrix} \quad \sigma_{22} = \sigma_{33} \tag{17}$$

The equations of motion for each constituent in a one-dimensional case are denoted by

For solid phase $$\frac{\partial q}{\partial X_1} = \rho_0^s \frac{\partial v_1^s}{\partial t} + \frac{\partial (nu)}{\partial X_1} + \Pi_1 \tag{18}$$

For fluid phase $$\frac{\partial(nu)}{\partial X_1}=\rho_0^f\frac{\partial v_1^f}{\partial t}-\Pi_1 \tag{19}$$

$$\Pi_1=-d(v_1^f-v_1^s), \tag{20}$$

where ρ_0^s is the initial mass density of the solid contiuum, ρ_0^f is the initial mass density of the fluid continuum, v_i is the component of the velocity vector and Π_i is the component of the interaction force vector.

In a case where the strain-rate is very high, it is reasonable that v_1^s is equal to v_1^f. Then, the equation of motion becomes

$$\frac{\partial q}{\partial X_1}=\rho_0\frac{\partial v_1}{\partial t}\qquad(\rho_0=\rho_0^s+\rho_0^f,\ v_1=v_1^s=v_1^f) \tag{21}$$

The relation between the strain-rate and the particle velocity is expressed by

$$-\frac{\partial\varepsilon_{11}}{\partial t}=\frac{\partial v_1}{\partial X_1} \tag{22}$$

Eqs. (15), (21) and (22) form the quasi-linear partial differential equations. The characteristics are therefore given by

$$dX_1=0,\ dX_1/dt=\pm\sqrt{\frac{E'}{\rho_0}}=\pm C \tag{23}$$

along which the following differential equations exist:

Along $dX_1=0$, $$d\varepsilon_{11}=\frac{1}{E'}dq+(\mu q-E\mu\varepsilon_{11}^{ve})\,dt+C_1\exp\left(\frac{m}{\sigma_{me}'}(q-q^{(s)})\right) \tag{24}$$

Along $dX_1/dt=\pm C$

$$dv_0=\mp\frac{1}{\rho_0 C}dq-\left[(\mu q-E\mu\varepsilon_{11}^{ve})+C_1\exp\left(\frac{m}{\sigma_{me}'}(q-q^{(s)})\right)\right]E'\,dt \tag{25}$$

For an elastic-viscoplastic material, the second terms of the right hand side of Eqs. (24) and (25) are eliminated.

Differential relations (*e.g.* Eqs. (24) and (25)) are integrated along the characteristics by Massau's method. At first, the one-dimensional stress wave propagation through the viscoelastic-viscoplastic body is examined.

The used parameters in the calculation are as follows.

$e_0=0.863$, $M^*=1.30$, $\lambda=0.127$, $\kappa=0.021$, $E'=1.4\times10^7(\mathrm{kg/m^2})$

$\rho_0=196.3(\mathrm{kg.\,sec^2/m^2})$, $\sigma_{me}'=2.0\times10^4(\mathrm{kg/m^2})$, $m=23.0$

$C_1=2\times10^{-5}(1/\mathrm{sec})$, $C_2/\gamma_2=20.0(\mathrm{kg/cm^2/sec})$, $k=0.5(=E/E')$

$E\mu=0.98\times10^2(1/\mathrm{sec})$

E and μ(viscocity coefficient) can be determined according to Akai & Hori[11] who concluded that the physical behavior of the soil is viscoelastic in the strain level of 10^{-4}—10^{-3}, and the soil can be assumed as a linear spring-Voigt model in a wide frequency range. The parameter k and the relaxation time $1/E\mu$ take the values of 1.0—0.5 and 1×10^{-2}—5×10^{-2}(sec), respectively.

e_0 is the initial void ratio, λ the slope of the e-$\ln\sigma_m'$ line of the consolidation test

and κ the slope of the e—$ln\ \sigma'_m$ line of the swelling test.

Fig. 9 shows the variation in the shape of the wave during the propagating

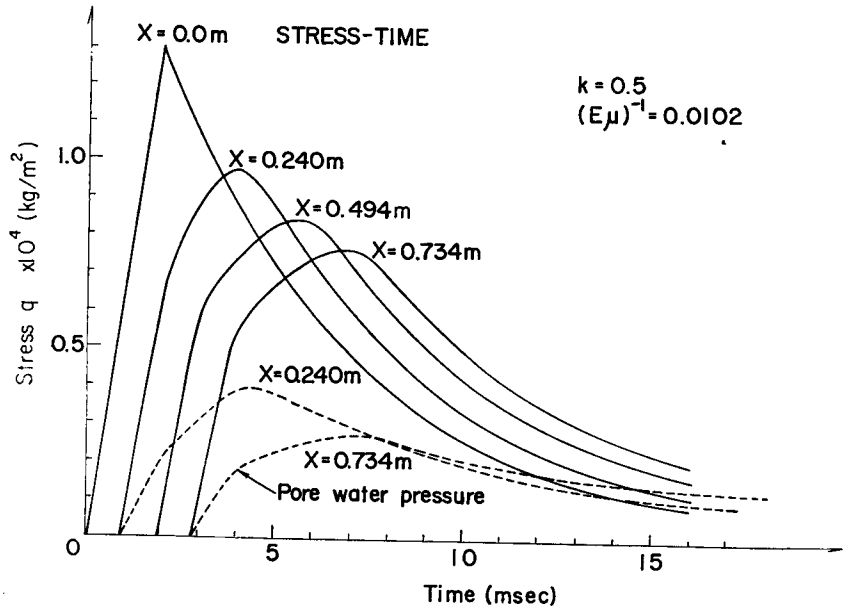

Fig. 9 Stress-time relationship and pore water pressure-time relationship.

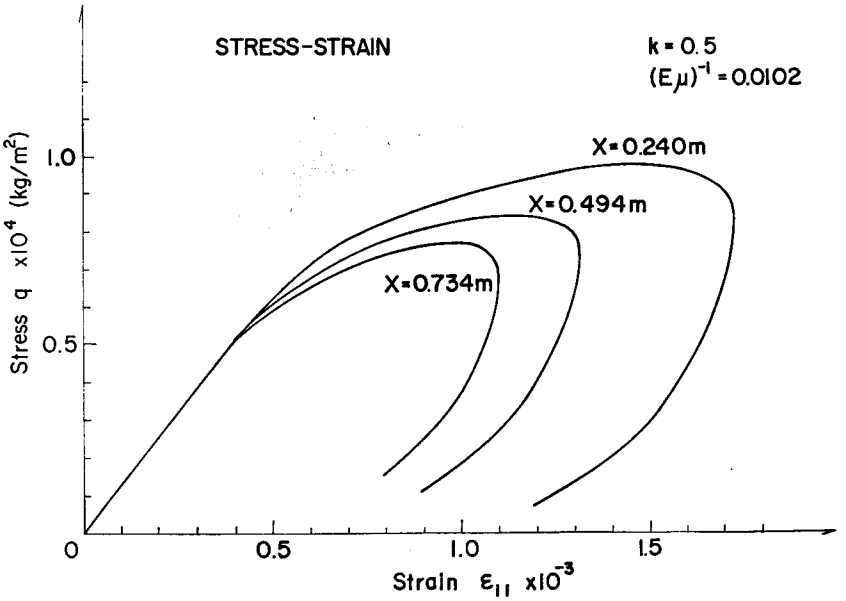

Fig. 10 Stress-strain relationship.

process. The shape of the wave in the neighbourhood of the peak stress becomes round as the wave advances. The rise time, which is defined as the difference in arrival times of the wave front and the peak stress, increases as the wave shape collapses. From Fig. 9, the induced attenuation of the peak stress is great in the first part of the rod, and then gradually becomes constant. Fig. 10 shows the stress-strain relations depicted during the wave propagation. The type of the stress-strain relation is bilinear in behavior and the hysteretic type dissipation is predominant. The area of the hysterisis loop becomes small as the maximum stress decreases. The viscoelastic effect of the Voigt type can be recognized, exhibiting a delayed elastic component of the strain. The dynamic stress path is shown in Fig. 11. Figs. 12 and 13 are the results in the case of neglecting the viscoelastic effect. From Fig. 13, it is shown that in the unloading part, the delayed elastic component of strain can not be recognized. Results without the viscoplastic effect are shown in Fig. 14 and 15, which correspond to the spring-Voigt model. The type of stress-strain relation is not bilinear. The collapse of the shape in the neighbourhood of the peak stress is smaller than that in Fig. 9. Figs. 16 and 17 show the experimental results of the stress-strain relation and the variation in the shape of the wave respectively. From the type of stress-strain relation and the variation of the wave shape, the viscoelastic -viscoplastic body can well express the behavior of cohesive soil during the wave propagation.

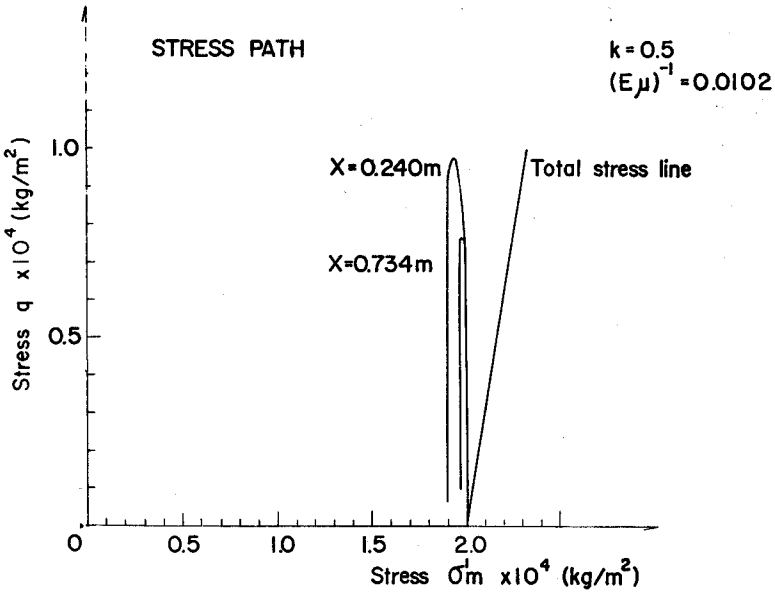

Fig. 11 Stress path.

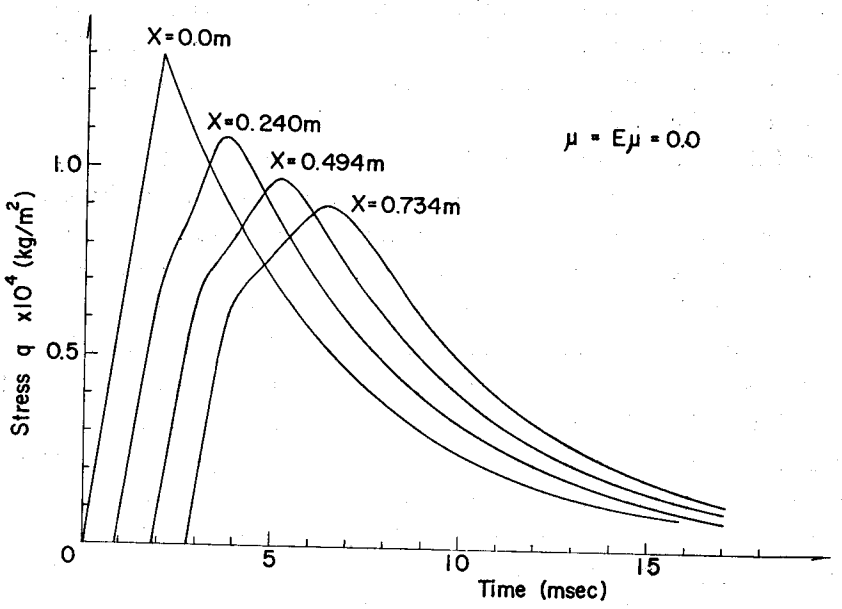

Fig. 12 Stress-time relationship.

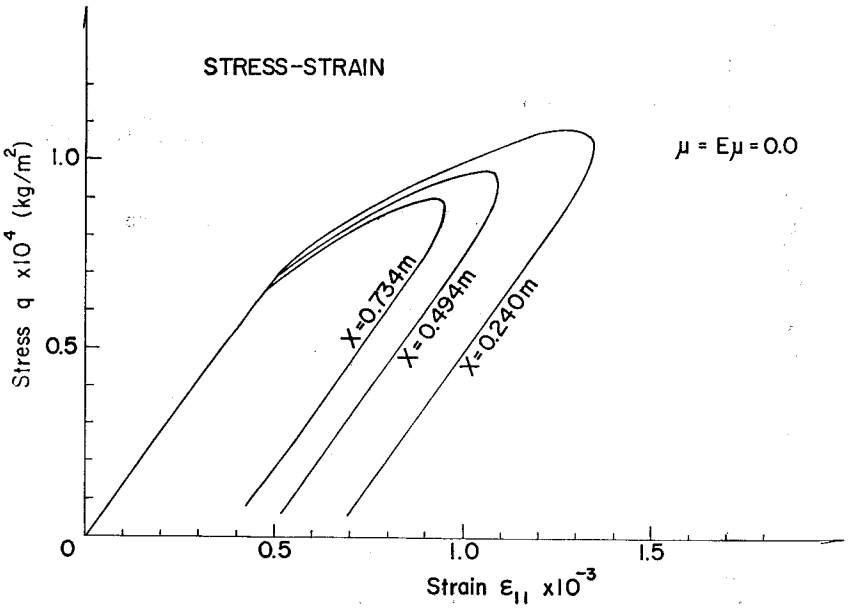

Fig. 13 Stress-strain relationship.

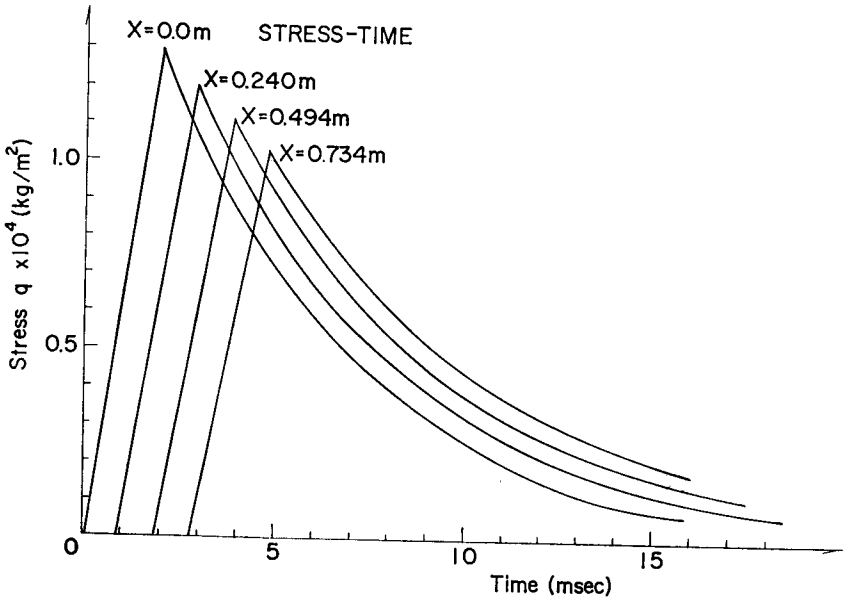

Fig. 14 Stress-time relationship.

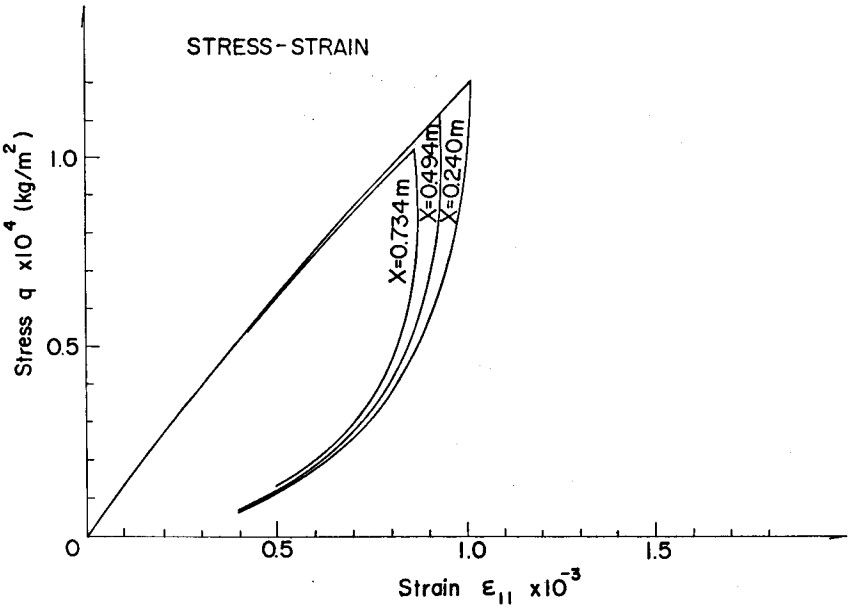

Fig. 15 Stress-strain relationship.

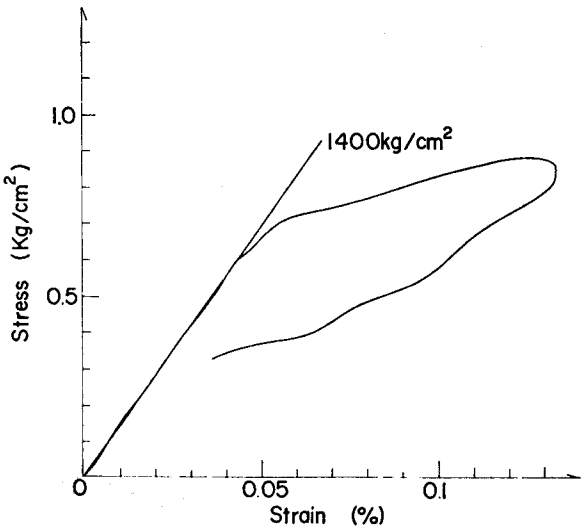

Fig. 16 Stress-strain relationship (experimental result).

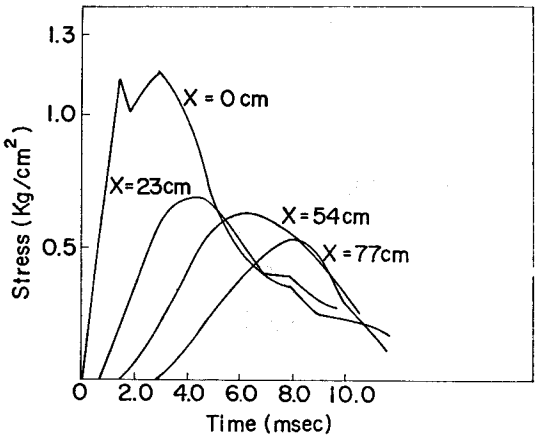

Fig. 17 Stress-time relationship (experimental result).

Generally, the parameters m and C_1, depend on the value of strain, and can be determined from the strain-rate controlled triaxial compression test as follows;

$$m=-1400\varepsilon_{11}+37 \qquad (\varepsilon_{11}\leq 10^{-2})$$

$$m=23 \qquad (\varepsilon_{11}\geq 10^{-2})$$

$$k=0.32,\ \frac{1}{E\mu}=1.03\times 10^{-2}\,(\text{sec}),\quad E'=1.73\times 10^{7}\,(\text{kg/m}^2)$$

$$C_1=[1.8\times 10^{-14}\times (10^2\times\varepsilon_{11})^{3.06}+10^{-17}]\exp(mq^{(s)}/\sigma'_{me}) \quad (\varepsilon_{11}\leq 10^{-2})$$

$$C_1=[1.8\times 10^{-14}+10^{-17}]\exp(mq^{(s)}/\sigma'_{me}) \quad (\varepsilon_{11}\geq 10^{-2})$$

$$C_2/\gamma_2=10\times C_1$$

The input surface wave approximately corresponds to the experimental result in Fig. 17.

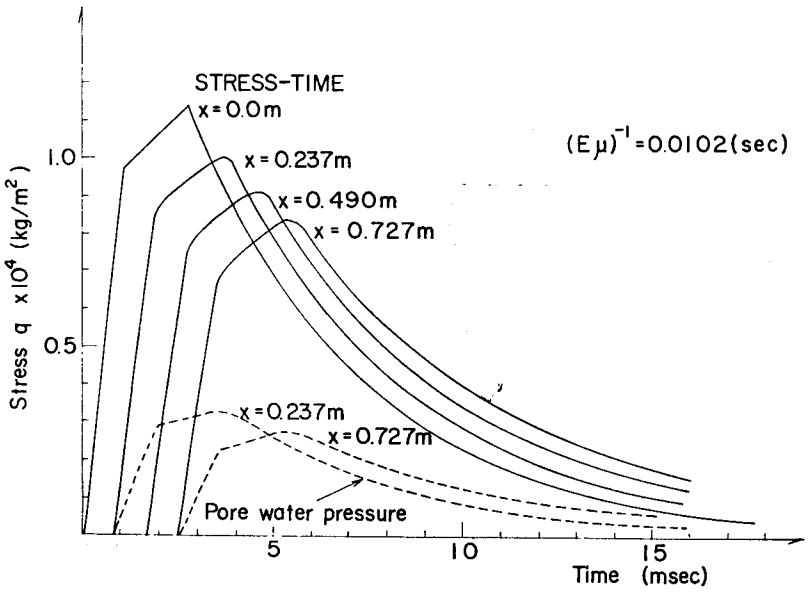

Fig. 18 Stress-time relationship and pore water pressure-time relationship.

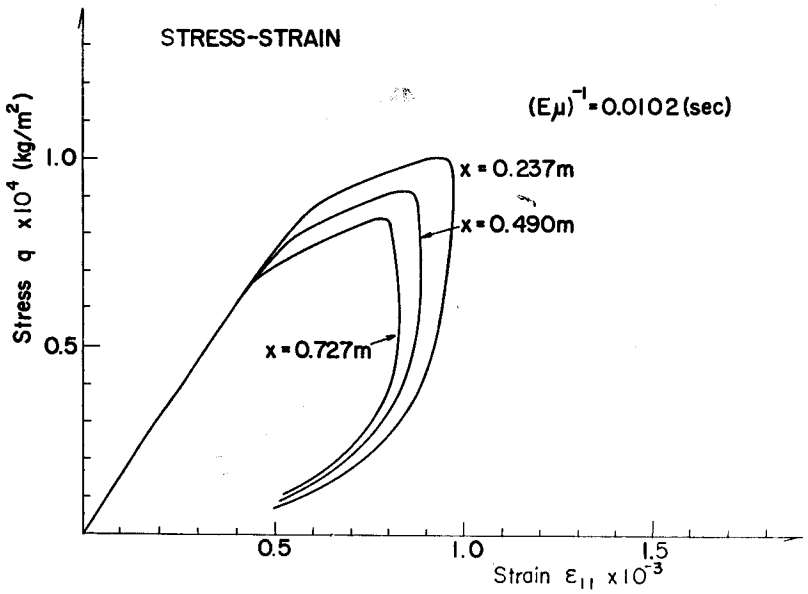

Fig. 19 Stress-strain relationship.

Fig. 18 shows the variation of the wave shape, and Fig. 19 shows the stress-strain relation. Comparing Fig. 19 with Fig. 16, the tendency of the stress-strain relation is similar in both cases. The peak stress attenuation at the first place of the bar in Fig. 17 is greater than that of the calculated result. This reason is that it is considered that an instantaneous plastic effect may have occurred in the experiment besides the non-instantaneous plastic effect expressed by Eq. 4. The calculated result of the pore water pressure is greater than the measured value in Table 2. In order to solve these difficulties, the three-dimensional analysis of the wave phenomena must be considered. In the present stage, it can be concluded that the combination of the viscoelastic model and viscoplastic model is very effective for interpreting the behavior of cohesive soil, judging from the strain rate constant triaxial compression test and the stress wave propagation test.

4. Conclusions

In this study, the one-dimensional stress wave propagation through cohesive soil is studied and the numerical calculation is done by using the proposed stress-strain relation of cohesive soil. The main conclusions obtained are as follows.

(1) The pore water pressure developed during the stress wave propagation through cohesive soil can be measured, using a pressure transducer with a needle-like tube filled with porous stone.

(2) The rate of the developement of the pore water pressure in the strain-rate constant triaxial compression test and in the stress wave propagation test can be predicted by the proposed stress-strain relation of cohesive soil.

(3) The proposed stress-strain relation is very effective for interpreting the behavior of cohesive soil.

References

1) Seaman, L., Stanford Reserch Inst., AD-632106, DASA1757, 19 (1966).
2) Vey, E. and L. V. Strauss, Proc. Int. Symp. on Wave Propagation and Dynamic Properties of Earth Materials, 575 (1967).
3) Akai, K. and M. Hori and T. Shimogami, Proc. of JSCE, No. 228, August, 99 (1974).
4) Akai, K. and F. Oka, Proc. of JSCE, No. 253, Sept., 109 (1976).
5) Oka, F. Proc. of JSCE, No. 272, Apr., 117 (1978).
6) Adachi, T. and M. Okano, Soils and Foundations, Vol. 14, No. 4, 55 (1974).
7) Richardson, A. M. and R. V. Whitman, Geotech., Vol. 13, No. 4, 310 (1963).
8) Yong, R. N. and R. D. Yapp, Vibrational Effects on Earthquakes on Soils and Foundations, ASTM STP, 450, 233 (1969).
9) Matsui, T., H. Ohara and T. Ito, Proc. of JSCE, No. 257, 41 (1977) (in Japanese)
10) Singh, A. and J. K. Mitchell, Journal of the Soil Mechanics and Foundation Division, A. S. C. E., Vol. 94, No. SM1, 21 (1968).
11) Akai, K. and M. Hori, Proc. of JSCE, No. 221, Jan., 81 (1974).